Research Square

Preprints are preliminary reports that have not undergone peer review.
They should not be considered conclusive, used to inform clinical practice,
or referenced by the media as validated information.

Boric Acid-Promoted Hydroxylation of Aryl Halides over a Magnetic SBA-15-Supported Pd-bis(NHC) Catalyst

Somayeh Fekri
University of Mohaghegh Ardabili
Yagoub Mansoori
ya_mansoori@uma.ac.ir

University of Mohaghegh Ardabili
Dolores Esquivel
Instituto Universitario de, Nanoquímica IUNAN, Universidad de Córdoba

Article

Keywords: Magnetic heterogeneous catalysis, Pd-NHC catalysis, aryl halide hydroxylation, mesoporous SBA-15, catalyst recyclability

Posted Date: November 13th, 2026

DOI: https://doi.org/10.21203/rs.3.rs-11521237/v1

License: This work is licensed under a Creative Commons Attribution 4.0 International License.
Read Full License

Additional Declarations: No competing interests reported.

Boric Acid-Promoted Hydroxylation of Aryl Halides over a Magnetic SBA-15-Supported Pd-bis(NHC) Catalyst

Somayeh Fekri,[1], Yagoub Mansoori,*[1, 2], Dolores Esquivel [3]

[1] *Department of Applied Chemistry, Faculty of Science, University of Mohaghegh Ardabili, Ardabil, Iran, 56199-11367. Tel: +98 45 31505205. Fax: +98 45 33514024.*

[2] *Nanoscience and Nanotechnology Research Group, University of Mohaghegh Ardabili, Ardabil, Iran, 56199-11367.*

[3] *Departamento de Química Orgánica, Instituto Universitario de, Nanoquímica IUNAN, Facultad de Ciencias, Universidad de Córdoba, Campus de Rabanales, Edificio Marie Curie, Córdoba E-14071, España.*

*Correspondence: ya_mansoori@uma.ac.ir

Abstract

Fe_3O_4@SBA-bis(NHC)-Pd(II) is a highly effective and magnetically removable catalyst for hydroxylating aryl halides. The substrates showed the effects of halogens, electronic effects, and steric effects. Aryl iodides and bromides were found to have higher reactivity than other substrates. The low leaching of palladium (0.03%) show that the catalysis is mainly due to the immobilized palladium species. The structural and textural stability of the catalyst during recycling was also confirmed. Magnetic separation allowed the catalyst to be readily recovered and reused for seven consecutive runs, retaining 79% of its initial activity. Overall, Fe_3O_4@SBA-bis(NHC)-Pd(II) is a reliable platform for recycling heterogeneous aryl halide hydroxylation processes.

Keywords: Magnetic heterogeneous catalysis; Pd-NHC catalysis; aryl halide hydroxylation; mesoporous SBA-15; catalyst recyclability

1. Introduction

Phenols are important structural motifs in a wide range of compounds used in agricultural chemicals [1], flavorings and colorings [2], food items [3], and medicines [4]. Industrial phenol production relies predominantly on the cumene process, which was introduced by Hock and Lang in 1944 [5]. In the cumene process, cumene is first produced from benzene and propene, and then converted to phenol. Despite its efficiency for large-scale production, the process is less suitable for synthesizing structurally complex phenols with sensitive functional groups.

The widespread occurrence and importance of phenols have driven the development of efficient and broadly applicable synthetic methods for their preparation. Transition-metal-catalyzed hydroxylation of aryl halides with hydroxide salts or surrogates is a widely used route to phenols [6-12]. However, the strong basicity and poor nucleophilicity of hydroxide limit its effectiveness in S_NAr reactions. Another strategy involves halogen-metal exchange followed by borylation and oxidative hydroxylation [13,14]. Although borylation is generally mild, the use of organolithium or Grignard reagents compromises functional-group tolerance. The subsequent oxidative step further narrows the substrate scope [15].

Photocatalytic hydroxylation has emerged as a promising approach for converting aryl halides to phenols under mild conditions. It was found by Sun *et al.* [16] that aryl chlorides could be hydroxylated with water as a source of hydroxyl and $UO_2(OAc)_2.2H_2O$ under blue LED irradiation. The reaction proceeds through single-electron transfer, hydrogen atom transfer, and oxygen transfer process steps. Photocatalytic methods, despite recent progress, remain constrained by several factors. These include the necessity for combined photoredox and

transition-metal catalysis, the requirement for complex ligands, the use of sacrificial electron donors, and extended irradiation periods. Additional challenges include a restricted substrate scope, catalyst deactivation, insufficient recyclability, and difficulties in scaling up [17-19].

Boric acid, a reagent characterized by its stability, affordability, and low toxicity, is widely employed in organic synthesis [20]. Notably, its application as a hydroxyl source in the palladium-catalyzed hydroxylation of (hetero)aryl halides has been documented only once. Interestingly, boric acid has been used only once as the hydroxyl source in the palladium-catalyzed hydroxylation of (hetero)aryl halides. Song and Wang [21] described the application of $Pd(OAc)_2$/tert-BuBrettPhos as a catalytic system for the hydroxylation of different (hetero)aryl halides. It exhibited excellent functional-group tolerance, including for sensitive functionalities.

Although boric acid is an effective hydroxylating agent, the catalytic system still requires a bulky phosphine ligand. Therefore, palladium catalysts modified with diverse ligand frameworks offer potential for expanding the scope of boric acid-mediated hydroxylation. *N*-heterocyclic carbenes (NHCs) represent a notable class of such ligands that has garnered significant research interest. Since their first introduction by Öfele *et al.* [22-24], NHCs have become versatile catalytic ligands. This observation is attributed to the strong electron-donating capacity, limited electron-accepting character, and inherent stability of these complexes. Palladium-*N*-heterocyclic carbene (NHC) complexes are effective catalysts for various transformations, including C-C and C-N bond formation [25,26], nitroaromatic reduction [27], and the transfer hydrogenation of alkynes and functionalized aromatics [28]. Their application in the hydroxylation of aryl halides has not been investigated, suggesting a potential area for expanding NHC-palladium catalysis.

The immobilization of homogeneous catalysts on solid supports facilitates catalyst recovery but often compromises catalytic activity [29-31]. Nanostructured supports can improve the

accessibility of active sites while maintaining the main advantages of heterogeneous catalysis [32]. SBA-15 and MCM-41, examples of mesoporous materials, exhibit high surface areas, ordered pore structures, and thermal stability, making them suitable catalyst supports. Their ordered mesoporous structures enhance reactant diffusion and active species distribution [33,34]. For instance, the work done by Havasi *et al.* [35] describes a palladium complex containing dithizone immobilized on MCM-41, which catalyzes the conversion of aryl halides to phenols.

Although mesoporous silica-supported catalysts are attractive for catalytic applications, getting them back from the reaction mixture usually needs filtration or centrifugation. The introduction of magnetic nanoparticles makes it possible to isolate them easily using magnetic isolation. are potential supports due to their superparamagnetic nature, large surface area, low cost, and easy isolation [36]. However, aggregation and oxidation limit their use. The mesoporous silica-coated magnetite nanoparticle may be useful in overcoming these limitations [37-39]. Consequently, Fe_3O_4@mesoporous silica nanocomposites have emerged as effective and magnetically recoverable solid supports for heterogeneous catalysis.

Our group has previously developed and applied Pd-NHC complexes supported on magnetic mesoporous silica (Fe_3O_4@SBA-15) in a variety of catalytic transformations, including cross-coupling, hydrodehalogenation, reduction, oxidation, amination, and carbonylation reactions [40-45]. Building on these studies, we report the first supported Pd-NHC catalyst for boric acid-mediated hydroxylation of aryl halides. The immobilization of the Pd-NHC complex onto magnetic mesoporous silica yielded the reusable Fe_3O_4@SBA-bis(NHC)-Pd(II) catalyst. It facilitated the conversion of aryl halides to phenols through hydroxylation in NMP in the presence of potassium carbonate. The catalyst was readily recovered by magnetic separation and reused for seven consecutive cycles with minimal loss of activity.

2. Experimental

2.1. General information

APTES was sourced from Exir (Austria), while Pluronic P123, tetraethoxysilane (TEOS), and $PdCl_2$ were purchased from Sigma-Aldrich. Unless otherwise stated, the remaining reagents and chemicals were obtained from Merck. All solvents used in this study were of laboratory grade and were dried prior to use following established literature procedures [46]. Magnetite nanoparticles and the palladium precursor *trans*-$[PdCl_2(SMe_2)_2]$ were synthesized following established literature procedures [47,48]. The supported Pd catalyst was subsequently prepared using the procedure described in our previous work [44]. A complete account of the catalyst synthesis, including the individual preparation and functionalization steps, is provided in the Supporting Information (SI).

2.2. Hydroxylation of aryl halides

A 10 mL thick-walled vial containing a magnetic stir bar was charged with aryl halide (0.50 mmol), Pd catalyst (30 mg, 1.60 mol% Pd), NMP (1.0 mL), potassium carbonate (0.207 g, 1.50 mmol), and boric acid (0.061 g, 0.75 mmol). The vial was purged with argon, sealed, and heated to 100 °C with magnetic stirring. The vial was flushed with argon gas, sealed, and then heated in an oil bath at 100 °C with magnetic stirring. Once the reaction had been completed-as monitored by TLC-the mixture was cooled to room temperature and diluted with water (3.0 mL). The catalyst was separated using a magnet, washed with ethyl acetate and acetone, and then dried in order to be used again. The aqueous layer was extracted with ethyl acetate, dried using sodium sulfate, and the solution was concentrated under reduced pressure. The crude product was purified by plate chromatography using a mixture of hexane and ethyl acetate as the eluent.

Phenol (2a): Colorless oil. (ºC): ^{1}H NMR (250 MHz, DMSO-d_6) δ 9.41 (s, 1H), 7.18 (t, J = 7.8 Hz, 2H), 6.90 - 6.72 (m, 3H). ^{13}C NMR (63 MHz, DMSO-d_6) δ 157.08, 129.06, 118.54, 114.98.

4-Aminophenol (2b): Pale yellow solid. m.p.(°C): 171-173 (Lit. 170-175 [49]). ^{1}H NMR (300 MHz, DMSO-d_6) δ 8.29 (bs, 1H), 6.56 - 6.42 (m, 4H), 4.43 (bs, 2H). ^{13}C NMR (75 MHz, DMSO-d_6) δ 148.36, 140.54, 115.65, 115.44.

4-Hydroxybenzoic acid (2c): White solid. m.p.(°C): 214-217 (Lit. 214-217 [50]). ^{1}H NMR (250 MHz, DMSO-d_6) δ 12.40 (s, 1H), 10.20 (s, 1H), 7.80 (d, J = 8.4 Hz, 2H), 6.81 (d, J = 8.4 Hz, 2H). ^{13}C NMR (63 MHz, DMSO-d_6) δ 166.93, 161.29, 131.26, 121.03, 114.80.

4-Hydroxyacetophenone (2d): White solid. m.p.(°C):105-107 (Lit. 106 [51]). ^{1}H NMR (250 MHz, DMSO-d_6) δ 10.34 (s, 1H), 7.80 (d, J = 8.1 Hz, 2H), 6.84 (d, J = 8.2 Hz, 2H), 2.43 (s, 3H). ^{13}C NMR (63 MHz, DMSO-d_6) δ 195.65, 161.70, 130.36, 128.25, 114.81, 25.81.

4-Hydroxybenzyl alcohol (2e): White solid. m.p.(°C): 120-122 (Lit. 118-119 [52]). ^{1}H NMR (250 MHz, DMSO-d_6) δ 9.22 (s, 1H), 6.93 (dd, J = 98.4, 7.8 Hz, 4H), 4.97 (s, 1H), 4.38 (s, 2H). ^{13}C NMR (63 MHz, DMSO-d_6) δ 155.88, 132.41, 127.81, 114.51, 62.52.

2-Hydroxybenzyl alcohol (2f): White solid. m.p.(°C): 82-84 (Lit. 82-84 [53]). ^{1}H NMR (250 MHz, DMSO-d_6) δ 9.31 (s, 1H), 7.29 (d, J = 6.6 Hz, 1H), 7.01 (s, 1H), 6.78 (d, J = 4.2 Hz, 2H), 4.98 (s, 1H), 4.52 (s, 2H). ^{13}C NMR (63 MHz, DMSO-d_6) δ 153.86, 128.14, 127.05, 118.37, 114.21, 58.00.

2-Aminophenol (2g): Pale yellow solid. m.p.(°C): 185-188 (Lit. 186-188 [54]). ^{1}H NMR (300 MHz, DMSO-d_6) δ 8.80 (s, 1H), 6.79 (t, J = 8.1 Hz, 1H), 6.07 - 5.92 (m, 3H), 4.79 (s, 2H). ^{13}C NMR (75 MHz, DMSO-d_6) δ 158.07, 149.75, 129.51, 105.56, 103.48, 101.08.

4-Nitrophenol (2h): Pale yellow solid. m.p.(°C):112-114 (Lit. 114 [55]). ^{1}H NMR (250 MHz, DMSO-d_6) δ 9.98 (s, 1H), 8.05 (d, J = 8.7 Hz, 2H), 6.85 (s, 2H). ^{13}C NMR (63 MHz, DMSO-d_6) δ 164.01, 138.98, 125.75, 115.40.

4-Hydroxybenzaldehyde (2i): White solid. m.p. (°C): 111-115 (Lit. 112-16 [56]). ^{1}H NMR (250 MHz, DMSO-d_6) δ 10.60 (s, 1H), 9.76 (s, 1H), 7.73 (d, J = 8.0 Hz, 2H), 6.91 (d, J = 8.2 Hz, 2H). ^{13}C NMR (63 MHz, DMSO-d_6) δ 190.58, 162.99, 131.77, 128.09, 115.50.

2-Nitrophenol (2j): Pale Yellow solid. m.p.(°C): 170-172 (Lit.171-172 [57]). ^{1}H NMR (250 MHz, DMSO-d_6) δ 10.92 (s, 1H), 7.85 (d, J = 8.2 Hz, 1H), 7.51 (t, J = 7.9 Hz, 1H), 7.02 (dd, J = 45.1, 8.1 Hz, 2H). ^{13}C NMR (63 MHz, DMSO-d_6) δ 157.05, 151.76, 136.45, 134.92, 124.79, 118.94, 118.72.

2-Hydroxybenzaldehyde (2k): Colorless oil. ^{1}H NMR (300 MHz, DMSO-d_6) δ 11.01 (s, 1H), 9.87 (s, 1H), 7.57 - 7.46 (m, 2H), 7.04 - 6.93 (m, 2H). ^{13}C NMR (75 MHz, DMSO-d_6) δ 196.16, 161.15, 136.52, 133.29, 120.23, 119.40, 117.13.

3-Aminophenol (2l): Pale yellow solid. m.p.(°C): 119-121 (Lit. 119-120 [57]). ^{1}H NMR (250 MHz, DMSO-d_6) δ 8.89 (s, 1H), 6.94 - 6.67 (m, 1H), 6.08 - 5.97 (m, 3H), 4.82 (s, 2H). ^{13}C NMR (63 MHz, DMSO-d_6) δ 157.71, 149.32, 129.25, 105.30, 103.23, 100.77.

1-Naphthol (2m): White solid. m.p.(°C):94-96 (Lit. 95 [58]). ^{1}H NMR (250 MHz, DMSO-d_6) δ 10.26 (s, 1H), 8.28 (s, 1H), 7.80 (s, 1H), 7.62 - 7.26 (m, 4H), 7.02 (s, 1H). ^{13}C NMR (63 MHz, DMSO-d_6) δ 153.02, 134.22, 127.11, 126.16, 125.79, 124.27, 121.81, 118.12, 107.85.

3. Results and discussion

3.1. Catalyst preparation

The Fe_3O_4@SBA-bis(NHC)-Pd(II) catalyst was synthesized according to the previously reported procedure [42]. Details on the characterization of Fe_3O_4@SBA-15 and the catalyst itself can be found in the Supporting Information (SI). The formation of Fe_3O_4@SiO_2 core-shell nanoparticles was done via hydrothermal co-precipitation of Fe(II)/Fe(III) ions in a water medium followed by silica coating [48]. The resulting magnetic core-shell nanoparticles were

subsequently incorporated into the mesoporous SBA-15 framework as reported by Wang *et al.* [59].

SEM studies showed that pure SBA-15 shows a highly ordered structure (Figure S1-a). On the other hand, Fe_3O_4@SBA-15 samples showed a well-dispersed coating of Fe_3O_4@SiO_2 core-shell structure around the mesoporous cavities (Figure S1-b). The results prove the incorporation of magnetic nanoparticles in the SBA-15 structure.

The magnetite was first treated successively with APTES, cyanuric chloride, sodium imidazolide, and finally 2-bromopyridine to give the bis-imidazolium precursor, Fe_3O_4@SBA-bis(PI). This was followed by metalation with *trans*-[$PdCl_2(SMe_2)_2$] at −78 °C yielded the Fe_3O_4@SBA-bis(NHC)-Pd(II) catalyst (Figure 1).

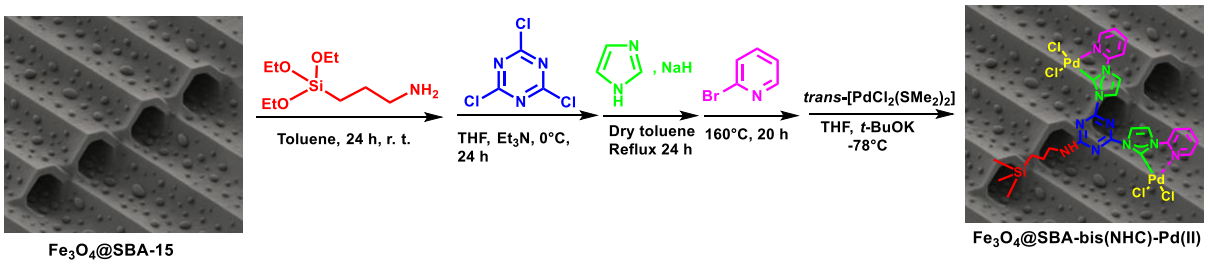


Figure 1. Synthetic pathway of Fe_3O_4@SBA-bis(NHC)-Pd(II).

The FT-IR spectrum of Fe_3O_4@SBA-bis(NHC)-Pd(II) shows pronounced changes relative to Fe_3O_4@SBA-15 (Figures S2-a,b). The C=N stretching bands of the imidazole and pyridine rings are observed at 1656 and 1576 cm^{-1}, respectively, confirming the successful incorporation of the NHC-containing ligand framework. Atomic absorption spectroscopy determined a Pd loading of 2.26 wt%, corresponding to 0.212 mmol g^{-1}.

The C 1s spectrum of Fe_3O_4@SBA-bis(PI) was fitted with three components at 284.6, 286.0, and 288.5 eV, assigned to C–H/C–C/C-ar, C–N, and C=N bonds, respectively (Figure S3-a). Upon Pd complexation, the C=N component shifted to 289.0 eV (Figure S3-b). The shift to

higher binding energy reflects a change in the electronic environment of the imine groups upon Pd coordination, supporting the formation of the Pd-imine complex.

The magnetic properties of the catalysts were evaluated by vibrating-sample magnetometry (Figure S4). The saturation magnetization (M_s) decreased only slightly from 6.0 emu g^{-1} for Fe_3O_4@SBA-15 to 5.9 emu g^{-1} for Fe_3O_4@SBA-bis(NHC)-Pd(II). Despite this minor decrease, the catalyst remained readily magnetically separable from the reaction medium.

N_2 adsorption-desorption analysis was used to probe the textural properties of the prepared materials, Table 1.

Table 1. Physical properties of the prepared materials.[a]

Sample	**S_{BET} (m^2 g^{-1})**	**Pore volume (cm^3 g^{-1})**
Fe_3O_4@SBA-15	620	1.23
Fe_3O_4@SBA-bis(NHC)-Pd(II)	164 (120)	0.26 (0.22)

[a] The values in the parenthesis refer to the measured parameters in the recovered catalysts after 6 cycles.

Fe_3O_4@SBA-15 exhibits a type IV isotherm with an H2-type hysteresis loop, characteristic of a mesoporous structure, Figure S5a-b [60]. Its BET surface area and total pore volume are 620 m^2 g^{-1} and 1.23 cm^3 g^{-1}, respectively. Upon functionalization of Fe_3O_4@SBA-15 with the Pd complex, these values decrease to 164 m^2 g^{-1} and 0.26 cm^3 g^{-1}, respectively. The BJH pore-size distribution also changes markedly after functionalization, Figure S5-b. The substantial reductions in surface area and pore volume, together with the decrease in pore diameter, support the successful immobilization of the Pd complex within the Fe_3O_4@SBA-15 framework.

3.2. Hydroxylation of aryl halides

The catalytic performance of Fe_3O_4@SBA-bis(NHC)-Pd(II) was evaluated using the hydroxylation of 4-bromoaniline to 4-aminophenol in the presence of boric acid as the model

reaction. The effects of solvent, base, boric acid loading, catalyst loading, and reaction temperature were systematically investigated. The results obtained from the optimizations are given in Table 2 and Figures 2a-c.

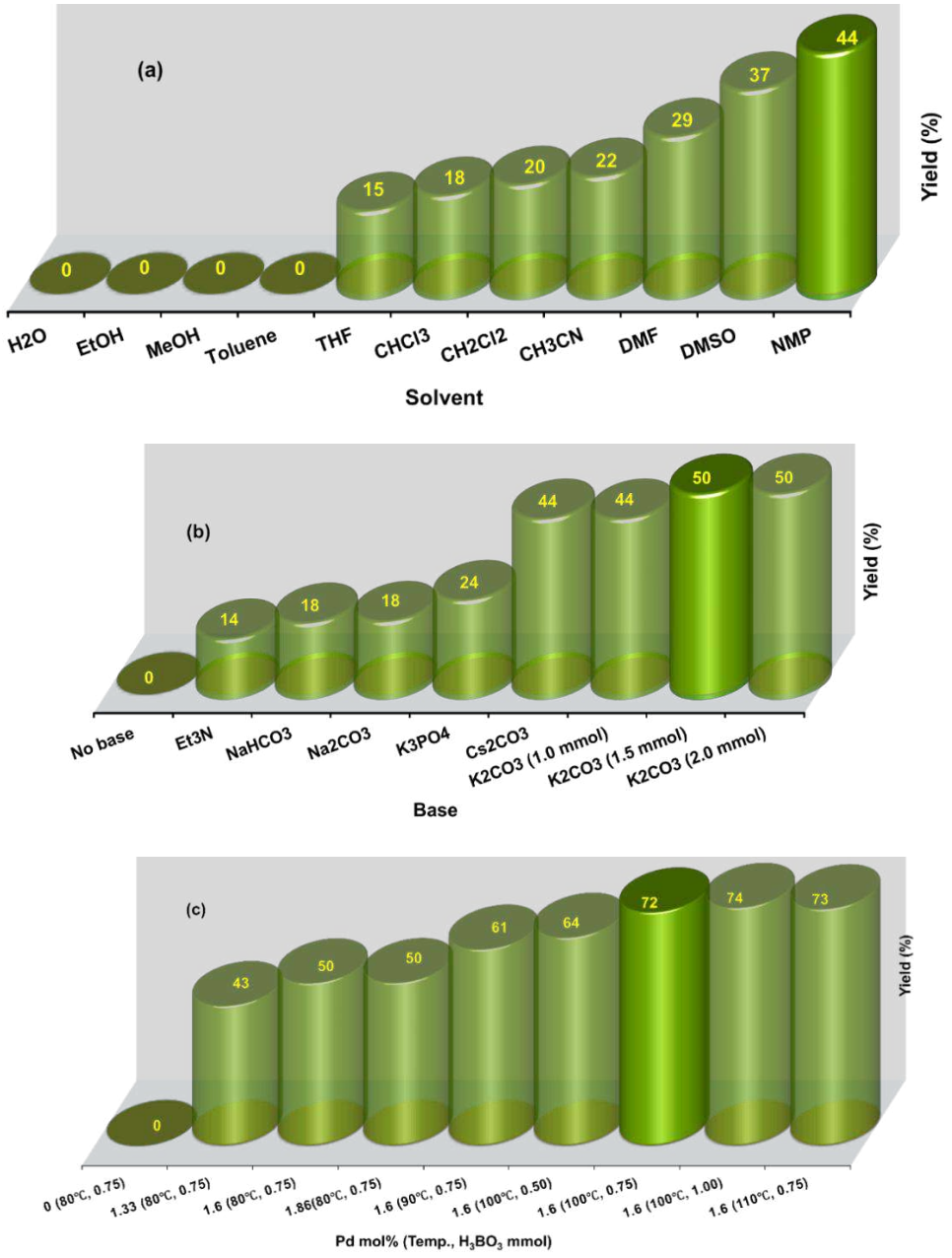
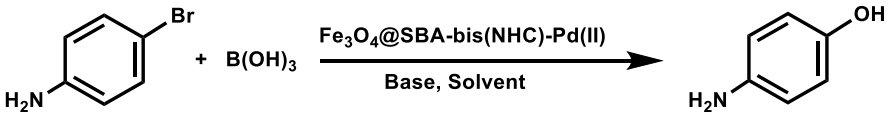


Figure 2. Optimization of the hydroxylation reaction conditions: 4-Bromoaniline (0.5 mmol), Solvent (1.0 mL), Pd(II) 1.6 mol%, reaction temperature 80°C, boric acid 0.75 mmol., and reaction time 24 h; a) Solvent: K_2CO_3 1.0 eq; b) Base; and c) Catalyst dosage, boric acid content, and reaction temperature.

There is no conversion in water, ethanol, methanol, and toluene (entries 1-4). NMP proved to be the best solvent with 44% yield (entry 11). The influence of the base was then investigated (entries 11 and 13-19).

Table 2. Optimization of conditions for the catalytic hydroxylation of 4-aminophenol [a,b].

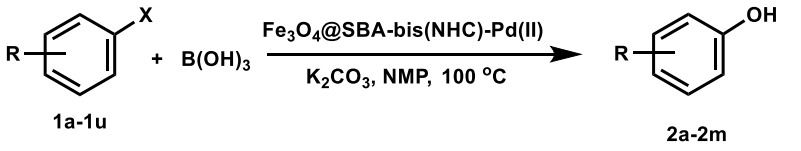


Entry	Solvent	Base (mmol)	Pd (mol%)/(mg)	Yield (%) [b]
1	H_2O	K_2CO_3	1.60/30	0
2	EtOH	K_2CO_3	1.60/30	0
3	MeOH	K_2CO_3	1.60/30	0
4	Toluene	K_2CO_3	1.60/30	0
5	THF	K_2CO_3	1.60/30	15
6	$CHCl_3$	K_2CO_3	1.60/30	18
7	CH_2Cl_2	K_2CO_3	1.60/30	20
8	CH_3CN	K_2CO_3	1.60/30	22
9	DMF	K_2CO_3	1.60/30	29
10	DMSO	K_2CO_3	1.60/30	37
11	NMP	K_2CO_3	1.60/30	44
12	NMP	No base	1.60/30	0
13	NMP	Et_3N	1.60/30	14
14	NMP	$NaHCO_3$	1.60/30	18
15	NMP	Na_2CO_3	1.60/30	18
16	NMP	K_3PO_4	1.60/30	24
17	NMP	Cs_2CO_3	1.60/30	44
18 [c]	NMP	K_2CO_3	1.60/30	50
19 [d]	NMP	K_2CO_3	1.60/30	50
20 [c]	NMP	K_2CO_3	No catalyst	0
21 [c]	NMP	K_2CO_3	[e] Pd-free pre-catalyst	0
22 [c]	NMP	K_2CO_3	1.33/25	43
23 [c]	NMP	K_2CO_3	1.86/35	50
24 [c, f]	NMP	K_2CO_3	1.6/30	61
25 [c, g]	**NMP**	**K_2CO_3**	**1.6/30**	**72**
26 [c, h]	NMP	K_2CO_3	1.6/30	73
27 [c, i]	NMP	K_2CO_3	1.6/30	64
28 [c, j]	NMP	K_2CO_3	1.6/30	74

Optimal reaction conditions are in bold. [a] Reaction conditions: 4-Bromoaniline (0.50 mmol), Boric acid 0.75 mmol, K_2CO_3 (1.0 mmol), Pd (1.6 mol%, 30 mg), Solvent (1.0 mL), reaction time 24 h, and temperature 80°C. [b] Isolated yields. [c] K_2CO_3 1.5 mmol. [d] K_2CO_3 2.0 mmol.[e] Pd free pre-catalyst 30 mg. [f] Reaction temperature 90°C. [g] Reaction temperature 100°C. [h] Reaction temperature 110°C. [i] $B(OH)_3$ 0.50 mmol. [j] Boric acid 1.0 mmol.

It was found that potassium carbonate (K_2CO_3, 1.5 equiv.) is the most efficient base, increasing the yield up to 50% (entry 18). Control experiments showed that no conversion occurred in the absence of either a base or a catalyst (Entries 12 and 20). Moreover, no conversion was observed when the Pd-free reagent was used instead of the Pd catalyst (Entry 21). Further optimizations involved the catalyst loading, boric acid, and reaction temperature. The maximum yield (72%) was obtained using 1.6 mol% Pd and 0.75 equiv. of boric acid at 100 °C (entry 25). Increasing the temperature to 110 °C and the boric acid loading to 1.0 equiv. had only a slight effect (entries 26 and 28).

A wide range of aryl halides underwent hydroxylation under the optimized conditions, Scheme 2. The reaction efficiency was strongly dependent on the halogen identity, electronic nature of the substituents, and substitution pattern.



1a-1u

2a-2m

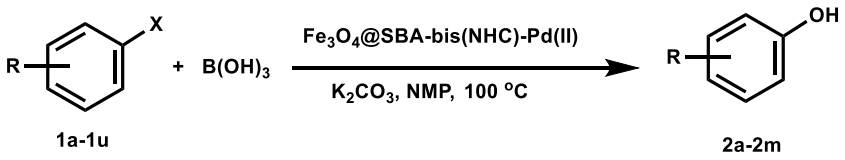
R = H	1a: X = I 1b: X = Br 1c: X = Cl
R = 4-NH_2	1d: X = Br 1e: X = Cl
R = 4-COOH	1f: X = Br 1g: X = Cl
R = 4-$COCH_3$	1h: X = Br 1i: X = Cl
R = 4-CH_2OH	1j: X = Br 1k: X = Cl
R = 2-CH_2OH	1l: X = Br 1m: X = Cl
R = 2-NH_2	1n: X = Br 1o: X = Cl
R = 4-NO_2	1p: X = Br
R = 4-CHO	1q: X = Br
R = 2-NO_2	1r: X = Br
R = 2-CHO	1s: X = Br
R = 3-NH_2	1t: X = Br
	1u: 1-Bromonaphthalene

2a: R = H
2b: R = 4-NH_2
2c: R = 4-COOH
2d: R = 4-$COCH_3$
2e: R = 4-CH_2OH
2f: R = 2-CH_2OH
2g: R = 2-NH_2
2h: R = 4-NO_2
2i: R = 4-CHO
2j: R = 2-NO_2
2k:R = 2-CHO
2l: 3-NH_2
2m: 1-Naphthol

Scheme 2. The hydroxylation reaction of aryl halides catalyzed by Fe_3O_4@SBA-bis(NHC)-Pd(II).

As shown in Table 3, the catalytic activity also depended on the nature of the halogen substituent. Yields of phenol were 56%, 47%, and 31% from iodobenzene **(1a)**, bromobenzene **(1b)**, and chlorobenzene **(1c)**, respectively.

Table 3. Hydroxylation of haloarenes.[a, b]



Entry	R	X	Product	Time (h)	Yield (%)/TOF (h^{-1}) × 10
1	H	I **(1a)**	**2a**	23	56/18
2		Br **(1b)**		24	47/15
3		Cl **(1c)**		24	31/10
4	4- NH_2	Br **(1d)**	**2b**	20	72/23
5		Cl **(1e)**		20	54/17
6	4-COOH	Br **(1f)**	**2c**	21	40/13
7		Cl **(1g)**		22	30/9
8	4-$COCH_3$	Br **(1h)**	**2d**	25	40/13
9		Cl **(1i)**		25	-/-
10	4-CH_2OH	Br **(1j)**	**2e**	25	40/13
11		Cl **(1k)**		26	33/10
12	2-CH_2OH	Br **(1l)**	**2f**	25	40/13
13		Cl **(1m)**		25	-/-
14	2-NH_2	Br **(1n)**	**2g**	20	62/19
15		Cl **(1o)**		23	49/15
16	4-NO_2	Br **(1p)**	**2h**	25	30/9
17	4-CHO	Br **(1q)**	**2i**	22	53/17
18	2-NO_2	Br **(1r)**	**2j**	25	21/7
19	2-CHO	Br **(1s)**	**2k**	22	46/14
20	3-NH_2	Br **(1t)**	**2l**	22	60/19
21	1-Naphthyl	Br **(1u)**	**2m**	25	33/10

[a] Reaction conditions: Arylhalide 0.5 mmol; K_2CO_3 1.5 mmol; $B(OH)_3$ 0.75 mmol; Pd mol% 1.6; and NMP 1.0 ml. [b] Isolated yields.

Reactivities are higher for aryl iodides and bromides, which can perhaps be attributed to a greater ease of palladium-mediated activation of the C-X bond. A trend for substituted

substrates was apparent too. The yield of **(2b)** with 4-bromoaniline **(1d)** was 72% whereas with 4-chloroaniline **(1e)** was 54%. The electronic nature of the substituents also influenced the reaction. Electron-rich starting materials seem to be the most reactive. E.g., 4-bromoaniline **(1d)** produces **(2b)** in 72% yield, compared to only 30% yield for the reduction of 4-bromonitrobenzene **(1p)** to **(2h)**. Carbonyls appear tolerant. 4-Bromobenzaldehyde **(1q)** produced **(2i)** in 53% yield, and 4-bromoacetophenone produced **(2d)** in 40% yield. Conversely, 4-chloroacetophenone **(1i)** gave no reaction. Steric effects were evident from the substitution pattern. Para isomers proved to be better than their ortho counterparts; for example, while **(1d)** and **(1p)** produced yields of 72% and 30%, respectively, **(1n)** and **(1r)** produced yields of 62% and 21% for **(1p)** and **(1r)**, respectively. Meta-substituted substrates showed moderate reactivity. Benzyl alcohol derivatives **(1j-1m)** and 2-bromonaphthalene **(1u)** were also reactive, affording the corresponding phenols in 33-40% yields. Thus, aryl iodides and bromides, particularly electron-rich and less sterically hindered aromatic substrates, showed the highest reactivity.

As shown in Figure 3, the Fe_3O_4@SBA-bis(NHC)-Pd(II) catalyst was active for seven consecutive hydroxylation reactions of 4-bromoaniline.

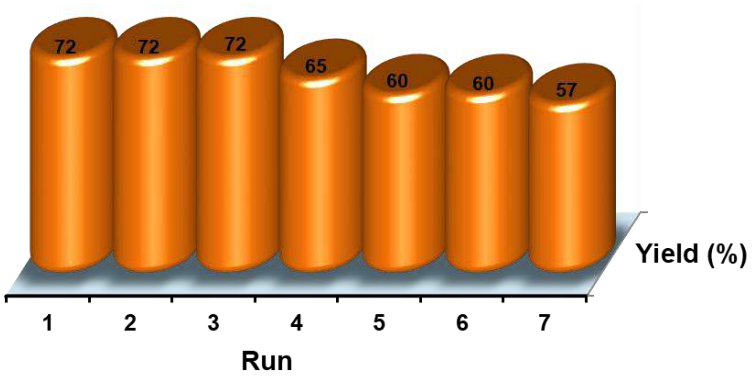


Figure 3. Recycling of Fe_3O_4@SBA-bis(NHC)-Pd(II) in the hydroxylation of 4-bromoaniline.

The yield was steady at 72% for the first three runs and then gradually decreased to 57% at the seventh run. This slight decrease in activity may be attributed to gradual catalyst deactivation upon repeated use. Nevertheless, the catalyst retained 79% of its initial activity after seven consecutive runs.

3.3. Assessment of palladium leaching and catalyst stability

Following catalyst separation, an aliquot of the 4-bromoaniline hydroxylation reaction mixture was analyzed for Pd leaching. Only 2.1×10^{-6} mmol of Pd was detected, corresponding to 0.03% leaching. The negligible Pd loss confirms strong metal immobilization and high catalyst stability under the reaction conditions.

The FT-IR spectra of the fresh catalyst and the catalyst recovered after seven hydroxylation runs are shown in Figure 4.

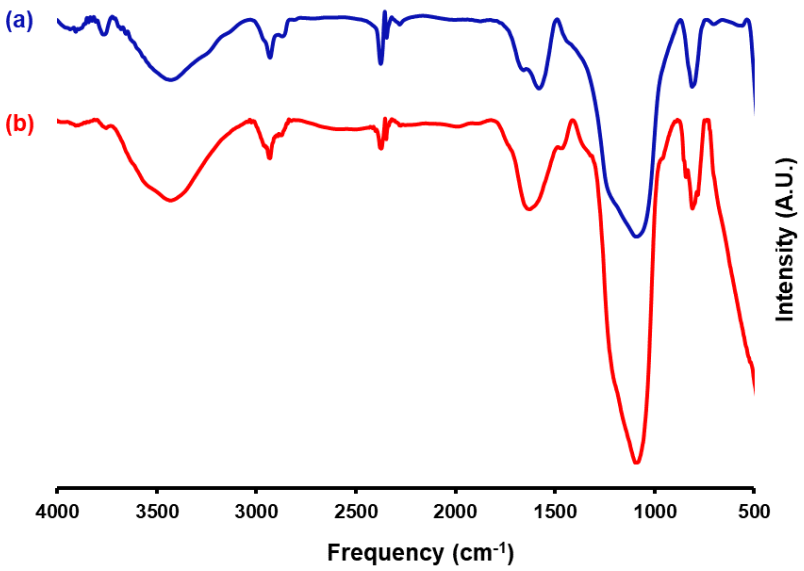


Figure 4. FT-IR spectra of (a) fresh and (b) recovered catalyst after seven runs.

The recovered catalyst retains the characteristic vibrational features of the fresh material. No appreciable band shifts or new absorptions are observed. Only minor changes in band

intensity are evident after seven runs. The preserved spectral profile confirms the structural integrity of the catalyst and its surface functionalities throughout repeated catalytic cycles.

The textural characteristics of the fresh catalyst and the catalyst recovered after six hydroxylation cycles were evaluated by N_2 adsorption-desorption analysis (Figure 5; Table 1).

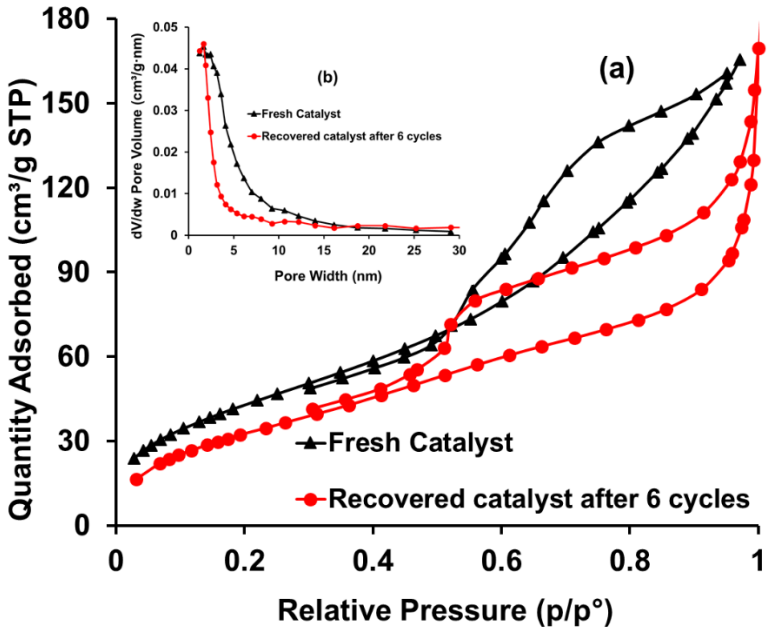


Figure 5. a) Nitrogen adsorption-desorption isotherms and b) pore size distribution of the fresh and the recovered Pd(II) catalyst after seven runs.

The isotherms of both samples were similar, indicating that the mesoporous structure was retained in the used catalyst. BET surface area was reduced from 164 to 120 $m^2\ g^{-1}$, and total pore volume was reduced from 0.26 to 0.22 $cm^3\ g^{-1}$. These modest changes demonstrate the high textural stability of the catalyst under the reaction conditions.

Conclusion

The Fe_3O_4@SBA-bis(NHC)-Pd(II) catalyst combines magnetic recyclability with a stable mesoporous structure. The leaching test confirmed negligible Pd leaching, with only 0.03% of

the Pd released into the reaction medium. The catalyst did not lose its distinct spectroscopic and textural characteristics during the reusability study. Only small variations in the specific surface area and total pore volume occurred during six cycles of the reaction. The catalyst retained 79% of its initial activity over seven consecutive hydroxylation cycles, demonstrating good stability. The magnetic SBA-15 support enabled easy catalyst separation and effective immobilization of the Pd species.

References

1 Benito-Román, Ó., Melgosa, R., Benito, J. M. & Sanz, M. T. Identification of Phenolics and Structural Compounds of Different Agro-Industrial By-Products. *Agriculture* **15**, 299, doi:10.3390/agriculture15030299 (2025).

2 An, J.-P., Kim, D., Song, X., Chater, J. M., Heinitz, C. C. & Wang, Y. Uncovering the biosynthetic pathways of key flavor and color compounds in pomegranate using pathway-based metabolomics. *RSC Adv.* **15**, 22831-22842, doi:10.1039/D5RA00511F (2025).

3 Li, W., Zogona, D. & Beta, T. in *Natural Products: Phytochemistry, Botany, Metabolism of Alkaloids, Phenolics and Terpenes* (eds Kishan Gopal Ramawat & Jean-Michel Mérillon) 1-36 (Springer Berlin Heidelberg, 2025).

4 Dunker, C., Schlegel, K. & Junker, A. Phenol (bio)isosteres in drug design and development. *Arch. Pharm.* **358**, e2400700, doi:https://doi.org/10.1002/ardp.202400700 (2025).

5 Hock, H. & Lang, S. Autoxydation von Kohlenwasserstoffen, IX. Mitteil.: Über Peroxyde von Benzol-Derivaten. *Ber. Dtsch. Chem. Ges.* **77**, 257-264, doi:https://doi.org/10.1002/cber.19440770321 (1944).

6 Alonso, D. A., Nájera, C., Pastor, I. M. & Yus, M. Transition-Metal-Catalyzed Synthesis of Hydroxylated Arenes. *Chem. Eur. J.* **16**, 5274-5284, doi:https://doi.org/10.1002/chem.201000470 (2010).

7 Xia, S., Gan, L., Wang, K., Li, Z. & Ma, D. Copper-Catalyzed Hydroxylation of (Hetero)aryl Halides under Mild Conditions. *J. Am. Chem. Soc.* **138**, 13493-13496, doi:10.1021/jacs.6b08114 (2016).

8 Fier, P. S. & Maloney, K. M. Synthesis of Complex Phenols Enabled by a Rationally Designed Hydroxide Surrogate. *Angew. Chem. Int. Ed.* **56**, 4478-4482, doi:https://doi.org/10.1002/anie.201700244 (2017).

9 Amal Joseph, P. J. & Priyadarshini, S. Copper-Mediated C–X Functionalization of Aryl Halides. *Org. Process Res. Dev.* **21**, 1889-1924, doi:10.1021/acs.oprd.7b00285 (2017).

10 Hariprasad, B. S. & Ganesh Babu, S. Supremacy of in-situ doping over surface loading technique for the preparation of alkali metal-promoted tellurates as efficient reusable catalysts to approach hydroxylation and dehalogenation of aryl halides. *Appl. Surf. Sci.* **669**, 160503, doi:https://doi.org/10.1016/j.apsusc.2024.160503 (2024).

11 Widlicka, D. W., Singer, R. A., Hotham, I., Bernhardson, D. J. & Grosslight, S. Copper-Catalyzed Hydroxylation of Aryl Halides Using Hydroxypicolinamide Ligands. *Org. Process Res. Dev.* **28**, 2732-2742, doi:10.1021/acs.oprd.4c00108 (2024).

12 Jones, G. A., Beshara, M., Levin, J. E., Garcevic, A. R., Rosiles-Dueñas, D. G., Saleh, Y. A. & Schultz, E. E. Pd-Catalyzed Hydroxylation of Aryl Halides under Air and in Eco-Friendly Solvent. *ACS Omega* **10**, 52814-52819, doi:10.1021/acsomega.5c06966 (2025).

13 Wagh, R. B. & Nagarkar, J. M. Facile and effective approach for oxidation of boronic acids. *Tetrahedron Lett.* **58**, 4572-4575, doi:https://doi.org/10.1016/j.tetlet.2017.10.059 (2017).

14 Liu, X., Li, D., Li, G., Wei, M., Yuan, S., Yang, M., He, L., Chen, S., Li, Z., Gao, L., Wang, G. & Li, S. Organometallic-type reactivity of stable organoboronates for selective (hetero)arene C−H/C-halogen borylation and beyond. *Nat. Commun.* **16**, 5458, doi:10.1038/s41467-025-60674-9 (2025).

15 Webb, K. S. & Levy, D. A facile oxidation of boronic acids and boronic esters. *Tetrahedron Lett.* **36**, 5117-5118, doi:https://doi.org/10.1016/0040-4039(95)00963-D (1995).

16 Sun, M., Bai, L., Li, C. & Jiang, X. From aryl chlorides to phenols: Photouranium-catalyzed hydroxylation via water splitting. *Chem Catal.* **4**, doi:10.1016/j.checat.2024.101027 (2024).

17 Skubi, K. L., Blum, T. R. & Yoon, T. P. Dual Catalysis Strategies in Photochemical Synthesis. *Chem. Rev.* **116**, 10035-10074, doi:10.1021/acs.chemrev.6b00018 (2016).

18 Gisbertz, S., Reischauer, S. & Pieber, B. Overcoming limitations in dual photoredox/nickel-catalysed C–N cross-couplings due to catalyst deactivation. *Nat. Catal.* **3**, 611-620, doi:10.1038/s41929-020-0473-6 (2020).

19 He, C., Zhou, X., Liu, W., Gu, S., Wu, X., Li, J., Zheng, M., Zhong, Y.-W., Wang, X. & Zhu, Y. Recent Advances in Activation of Aryl Halides over Organic and MOF-Based Semiconductor Photocatalysts: Mechanisms, Strategies, and Challenges. *ACS Catal.* **16**, 7920-7943, doi:10.1021/acscatal.6c01192 (2026).

20 Pal, R. Boric acid in organic synthesis: scope and recent developments. *ARKIVOC* **2018**, 346-371, doi:10.24820/ark.5550190.p010.462 (2018).

21 Song, Z.-Q. & Wang, D.-H. Palladium-Catalyzed Hydroxylation of Aryl Halides with Boric Acid. *Org. Lett.* **22**, 8470-8474, doi:10.1021/acs.orglett.0c03069 (2020).

22 Wanzlick, H.-W. & Schönherr, H.-J. Direct Synthesis of a Mercury Salt-Carbene Complex. *Angew. Chem. Int. Ed.* **7**, 141-142, doi:10.1002/anie.196801412 (1968).

23 Öfele, K. 1,3-Dimethyl-4-imidazolinyliden-(2)-pentacarbonylchrom ein neuer übergangsmetall-carben-komplex. *J. Organomet. Chem.* **12**, P42-P43, doi:https://doi.org/10.1016/S0022-328X(00)88691-X (1968).

24 Arduengo, A. J., Harlow, R. L. & Kline, M. A stable crystalline carbene. *J. Am. Chem. Soc.* **113**, 361-363, doi:10.1021/ja00001a054 (1991).

25 Cervantes-Reyes, A., Malpica-Calderón, R., Valdés, H. & Morales-Morales, D. Purine-derived N-heterocyclic carbene metal complexes: catalytic applications and reactivity. *Dalton Trans.* **55**, 7752-7776, doi:10.1039/d6dt00012f (2026).

26 Muniyappan, N. & Budagumpi, S. Recent advances in PEPPSI–themed palladium NHC complexes: Applications ranging from homogeneous catalysis to electrocatalysis. *Inorg. Chim. Acta* **589**, 122915, doi:https://doi.org/10.1016/j.ica.2025.122915 (2026).

27 Sobhani, S., Chahkamali, F. O. & Sansano, J. M. A new bifunctional heterogeneous nanocatalyst for one-pot reduction-Schiff base condensation and reduction–carbonylation of nitroarenes. *RSC Adv.* **9**, 1362-1372, doi:10.1039/C8RA10212K (2019).

28 Chen, H.-J., Chiu, C.-C., Wang, T., Lee, D.-S. & Lu, T.-J. Bis-NHC–Ag/$Pd(OAc)_2$ Catalytic System Catalyzed Transfer Hydrogenation Reaction. *Catalysts* **11**, 8 (2021).

29 He, Y., Zhou, J., Li, H., Deng, L. & Gao, J. Application of heterogeneous catalysts in the preparation of bio-based platform compound 5-hydroxymethylfurfural. *Bioresour. Bioprocess.* **12**, 55, doi:10.1186/s40643-025-00894-5 (2025).

30 Fathinejad, M., Mansoori, Y., Fekri, S., Akinay, Y. & Çetin, T. Efficient CO-free carbonylation of aryl halides catalyzed by SBA-15-supported Pd-1,10-phenanthroline. *Sci. Rep.*, doi:10.1038/s41598-026-52237-9 (2026).

31 Ghahramani, F., Mansoori, Y., Akinay, Y. & Çetin, T. SBA-15-supported copper(II)–2-hydrazinopyridine complex as an efficient reusable catalyst for the selective monoarylation of ammonia. *Sci. Rep.* **16**, 11167, doi:10.1038/s41598-026-39959-6 (2026).

32 Ahmad, H. & Hossain, M. K. Supported nanocatalysts: recent developments in microwave synthesis for application in heterogeneous catalysis. *Mater. Adv.* **3**, 859-887, doi:10.1039/D1MA00840D (2022).

33 Tahmasbi, B. & Ghorbani-Choghamarani, A. Magnetic MCM-41 nanoparticles as a support for the immobilization of a palladium organometallic catalyst and its application in C–C coupling reactions. *New J. Chem.* **43**, 14485-14501, doi:10.1039/C9NJ02727K (2019).

34 Nurwita, A., Stawicka, K. & Trejda, M. SBA-15 Type Mesoporous Silica Modified with Vanadium as a Catalyst for Oxidative and Extractive Oxidative Desulfurization Processes. *Materials* **17**, 4041, doi:10.3390/ma17164041 (2024).

35 Havasi, F., Ghorbani-Choghamarani, A. & Nikpour, F. Pd-grafted functionalized mesoporous MCM-41: a novel, green and heterogeneous nanocatalyst for the selective synthesis of phenols and anilines from aryl halides in water. *New J. Chem.* **39**, 6504-6512, doi:10.1039/C5NJ01102G (2015).

36 Caballero-Mejía, B., Moliner, A., Escolástico, C., Hontoria, C., Mariscal-Sancho, I. & Pérez-Esteban, J. Use of magnetite nanoparticles and magnetic separation for the removal of metal(loid)s from contaminated mine soils. *J. Hazard. Mater.* **486**, 137081, doi:https://doi.org/10.1016/j.jhazmat.2024.137081 (2025).

37 Abbasi, Z., Mansoori, Y., Fekri, S., Akinay, Y. & Çetin, T. Magnetically retrievable 2-(2-Pyridyl)benzimidazole-Cu(I) on SBA-15@Fe_3O_4 for sodium Azide-Induced amination of Aryl halides. *Sci. Rep.* **15**, 27812, doi:10.1038/s41598-025-13073-5 (2025).

38 Sotoude, M., Mansoori, Y., Ghahramani, F. & Bezaatpour, A. Copper dendritic catalyst on magnetic SBA-15 for O-arylation of phenols via the Ullmann reaction. *J. Coord. Chem.* **78**, 2094-2111, doi:10.1080/00958972.2025.2545393 (2025).

39 Alfaifi, A. H., Almutib, E., Algethami, N., Jain, V., Roopashree, R., Kashyap, A., Jayabalan, K. & Ray, S. Application of a copper complex supported on magnetic nanoparticles loaded on SBA-15 for Suzuki reaction under green and mild conditions. *Res. Chem. Intermed.* **51**, 2897-2916, doi:10.1007/s11164-025-05580-x (2025).

40 Nuri, A., Mansoori, Y. & Bezaatpour, A. N-heterocyclic carbene–palladium(II) complex supported on magnetic mesoporous silica for Heck cross-coupling reaction. *Appl. Organomet. Chem.* **33**, e4904, doi:10.1002/aoc.4904 (2019).

41 Nuri, A., Mansoori, Y., Bezaatpour, A., Shchukarev, A. & Mikkola, J.-P. Magnetic Mesoporous SBA-15 Functionalized with a NHC Pd(II) Complex: An Efficient and Recoverable Nanocatalyst for Hiyama Reaction. *ChemistrySelect* **4**, 1820-1829, doi:doi:10.1002/slct.201803798 (2019).

42 Fekri, S., Mansoori, Y., Esquivel, D. & Navarro, M. A. A New Bis-(NHC)-P(II) Complex Supported on Magnetic Mesoporous Silica: An Efficient Pd(II) Catalyst for the Selective Buchwald-Hartwig Monoarylation of Ammonia. *ChemistrySelect* **8**, e202204378, doi:https://doi.org/10.1002/slct.202204378 (2023).

43 Fekri, S., Mansoori, Y. & Bezaatpour, A. Bis(NHC)-Pd(II) and Pd(0) complexes supported on magnetic SBA-15 for the selective aerobic oxidation of benzyl alcohols to benzaldehydes and reduction of nitroarenes. *J. Organomet. Chem.* **993**, 122724, doi:https://doi.org/10.1016/j.jorganchem.2023.122724 (2023).

44 Fekri, S. & Mansoori, Y. Supported Bis-(NHC)-Pd(II) complex: A phosphine-free catalyst supported on magnetic mesoporous silica for the CO-free carbonylation of aryl halides. *J. Organomet. Chem.* **1014**, 123193, doi:https://doi.org/10.1016/j.jorganchem.2024.123193 (2024).

45 Fekri, S., Mansoori, Y., Esquivel, D. & Navarro, M. A. Efficient Hydrodehalogenation of Aryl Halides Catalyzed by Bis(NHC)-Pd(II) Complex Supported on Magnetic Mesoporous Silica. *Catal. Lett.* **154**, 695-707, doi:10.1007/s10562-023-04319-w (2024).

46 Armarego, W. L. F. & Chai, C. L. L. *Purification of laboratory chemicals*. 5th edn, 370 (Butterworth-Heinemann, 2003).

47 Mansoori, Y., Khodayari, A., Banaei, A., Mirzaeinejad, M., Azizian-Kalandaragh, Y. & Pooresmaeil, M. Fe_3O_4-PVAc nanocomposites: surface modification of sonochemically prepared magnetite nanoparticles via chemical grafting of poly(vinyl acetate). *RSC Adv.* **6**, 48676-48683, doi:10.1039/c5ra26783h (2016).

48 Philipse, A. P., van Bruggen, M. P. B. & Pathmamanoharan, C. Magnetic silica dispersions: preparation and stability of surface-modified silica particles with a magnetic core. *Langmuir* **10**, 92-99, doi:10.1021/la00013a014 (1994).

49 Hassan, H. M. A. A Highly Efficient $Ga(OTf)_3$/KI-Catalysed Transformation of aryl azides to aryl amines using low catalyst loading. *J. Chem. Res.* **42**, 572-574, doi:10.3184/174751918x15404076150031 (2018).

50 Sang, D., Yue, H., Fu, Y. & Tian, J. Cleavage of Carboxylic Esters by Aluminum and Iodine. *J. Org. Chem.* **86**, 4254-4261, doi:10.1021/acs.joc.1c00034 (2021).

51 Meynen, V., Cool, P. & Vansant, E. F. Synthesis of siliceous materials with micro- and mesoporosity. *Microporous Mesoporous Mater.* **104**, 26-38, doi:https://doi.org/10.1016/j.micromeso.2006.12.003 (2007).

52 Wang, R., Tang, Y., Xu, M., Meng, C. & Li, F. Transfer Hydrogenation of Aldehydes and Ketones with Isopropanol under Neutral Conditions Catalyzed by a Metal–Ligand Bifunctional Catalyst [Cp*Ir(2,2′-bpyO)(H_2O)]. *J. Org. Chem.* **83**, 2274-2281, doi:10.1021/acs.joc.7b03174 (2018).

53 Li, H.-J., Wu, Y.-Y., Wu, Q.-X., Wang, R., Dai, C.-Y., Shen, Z.-L., Xie, C.-L. & Wu, Y.-C. Water-promoted ortho-selective monohydroxymethylation of phenols in the $NaBO_2$ system. *Org. Biomol. Chem.* **12**, 3100-3107, doi:10.1039/C4OB00228H (2014).

54 Rahimi, J., Taheri-Ledari, R., Niksefat, M. & Maleki, A. Enhanced reduction of nitrobenzene derivatives: Effective strategy executed by Fe_3O_4/PVA-10%Ag as a

versatile hybrid nanocatalyst. *Catal. Commun.* **134**, 105850, doi:https://doi.org/10.1016/j.catcom.2019.105850 (2020).

55 Mo, J., Xu, L. & Xiao, J. Ionic Liquid-Promoted, Highly Regioselective Heck Arylation of Electron-Rich Olefins by Aryl Halides. *J. Am. Chem. Soc.* **127**, 751-760, doi:10.1021/ja0450861 (2005).

56 Layek, K., Maheswaran, H., Arundhathi, R., Kantam, M. L. & Bhargava, S. K. Nanocrystalline Magnesium Oxide Stabilized Palladium(0): An Efficient Reusable Catalyst for Room Temperature Selective Aerobic Oxidation of Alcohols. *Adv. Synth. Catal.* **353**, 606-616, doi:https://doi.org/10.1002/adsc.201000591 (2011).

57 Ghamari Kargar, P., Ravanjamjah, A. & Bagherzade, G. A novel water-dispersible and magnetically recyclable nickel nanoparticles for the one-pot reduction-Schiff base condensation of nitroarenes in pure water. *J. Chin. Chem. Soc.* **68**, 1916-1933, doi:https://doi.org/10.1002/jccs.202100172 (2021).

58 Paul, R., Ali, M. A. & Punniyamurthy, T. Copper-Catalyzed Hydroxylation of Aryl Halides with Tetrabutylammonium Hydroxide: Synthesis of Substituted Phenols and Alkyl Aryl Ethers. *Synthesis* **2010**, 4268-4272, doi:10.1055/s-0030-1258965 (2010).

59 Wang, S., Wang, K., Dai, C., Shi, H. & Li, J. Adsorption of Pb^{2+} on amino-functionalized core–shell magnetic mesoporous SBA-15 silica composite. *Chem. Eng. J.* **262**, 897-903, doi:https://doi.org/10.1016/j.cej.2014.10.035 (2015).

60 Sing, K. S. W. Reporting physisorption data for gas/solid systems with special reference to the determination of surface area and porosity (Recommendations 1984). *Pure Appl. Chem.* **57**, 603-619 (1985).

Funding

We extend our deepest gratitude for the generous financial support provided by the Graduate Council of the University of Mohaghegh Ardabili (Iran, Grant No. 99/D/13/25296).

Author contributions

Somayeh Fekri: Methodology, investigation, formal analysis, conceptualization, data curation, writing original draft. Yagoub Mansoori: conceptualization, data curation, writing - review & editing, resources, supervision, funding acquisition. Dolores Esquivel: XPS analysis and conceptualization.

Declaration of interest

The authors declare no competing interests.

Declaration of generative AI and AI-assisted technologies in the writing process

During the preparation of this work, the author(s) used ChatGPT in order to improve readability and language. After using this tool or service, the author(s) reviewed and edited the content as needed and take(s) full responsibility for the content of the publication.

Data availability

The datasets generated and/or analysed during the current study are available in the ScienceDB repository https://www.scidb.cn/en/anonymous/dWF5aU1q